Ocean Sci., 5, 421–433, 2009
www.ocean-sci.net/5/421/2009/

Ocean Science

Adjustment of the basin-scale circulation at 26° N to variations in Gulf Stream, deep western boundary current and Ekman transports as observed by the Rapid array

H. L. Bryden[1], **A. Mujahid**[1,2], **S. A. Cunningham**[1], **and T. Kanzow**[1,3]

[1]National Oceanography Centre, Empress Dock, Southampton SO14 3ZH, UK
[2]Universiti Malaysia Sarawak, 94300 Kota Samarahan, Sarawak, Malaysia
[3]Leibniz-Institut für Meereswisschenschaften, Düsternbrooker Weg 20, 24105 Kiel, Germany

Received: 30 March 2009 – Published in Ocean Sci. Discuss.: 30 April 2009
Revised: 11 September 2009 – Accepted: 11 September 2009 – Published: 19 October 2009

Abstract. The Rapid instrument array across the Atlantic Ocean along 26° N provides unprecedented monitoring of the basin-scale circulation. A unique feature of the Rapid array is the combination of full-depth moorings with instruments measuring temperature, salinity, pressure time series at many depths with co-located bottom pressure measurements so that dynamic pressure can be measured from surface to bottom. Bottom pressure measurements show a zonally uniform rise (and fall) of bottom pressure of 0.015 dbar on a 5 to 10 day time scale, suggesting that the Atlantic basin is filling and draining on a short time scale. After removing the zonally uniform bottom pressure fluctuations, bottom pressure variations at 4000 m depth against the western boundary compensate instantaneously for baroclinic fluctuations in the strength and structure of the deep western boundary current so there is no basin-scale mass imbalance resulting from variations in the deep western boundary current. After removing the mass compensating bottom pressure, residual bottom pressure fluctuations at the western boundary just east of the Bahamas balance variations in Gulf Stream transport. Again the compensation appears to be especially confined close to the western boundary. Thus, fluctuations in either Gulf Stream or deep western boundary current transports are compensated in a depth independent (barotropic) manner very close to the continental slope off the Bahamas. In contrast, compensation for variations in wind-driven surface Ekman transport appears to involve fluctuations in both western basin and eastern basin bottom pressures, though the bottom pressure difference fluctuations appear to be a factor of 3 too large, perhaps due to an inability to resolve small bottom pressure fluctuations after removal of larger zonal average, baroclinic, and Gulf Stream pressure components. For 4 tall moorings where time series dynamic height (geostrophic pressure) profiles can be estimated from sea surface to ocean bottom and bottom pressure can be added, there is no general correlation between surface dynamic height and bottom pressure. Dynamic height on each mooring is strongly correlated with sea surface height from satellite observations and the variability in both dynamic height and satellite sea surface height decrease sharply as the western boundary is approached.

Correspondence to: H. L. Bryden
(h.bryden@noc.soton.ac.uk)

1 Introduction

The extensive Rapid instrument array deployed across the Atlantic at 26° N (Kanzow et al., 2008) provides a unique opportunity to examine the dynamics of the large-scale ocean circulation. 26° N was selected as the location for monitoring the Atlantic meridional overturning circulation for several reasons. First, at 26° N, the Gulf Stream is confined to flow through Florida Straits and its transport has been measured there by a subsea electromagnetic cable nearly continuously since 1981 (Baringer and Larsen, 2001). Secondly, the bathymetry near the western boundary of the mid-ocean section at the Bahamas is relatively simple: there is a very steep continental slope from the reef at Abaco to a depth of 4000 m at an offshore distance of only 23 km. In addition, there is a small escarpment just north of 26.5° N with a depth of about 1500 m (see detailed bathymetry near the western boundary in Fig. 2 of Johns et al., 2008) that deflects the deep western boundary current offshore so that we can deploy a tall deep water mooring at 26.5° N in its shadow, out of the strong depth-independent deep boundary current flow that would normally make the uppermost instruments dip down substantially. Thirdly, 26° N is a zone of relatively

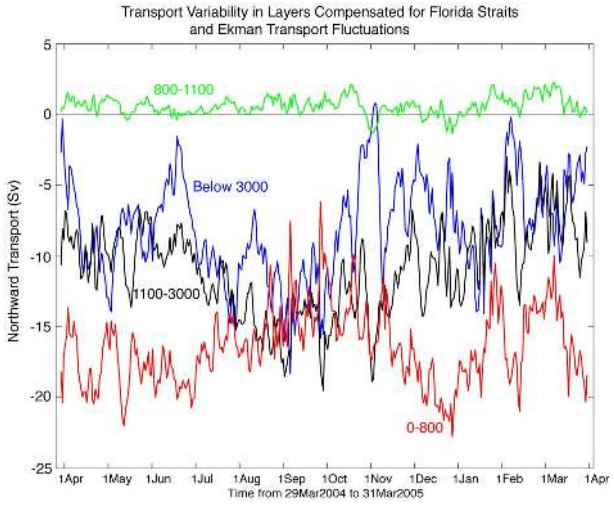

Fig. 1. Year-long time series of layer transports for thermocline recirculation (0 to 800 m depth, red), intermediate water (800 to 1100 m, green), upper North Atlantic Deep Water (1100 to 3000 m, black) and lower North Atlantic Deep Water (below 3000 m, blue). Negative transports correspond to southward flow.

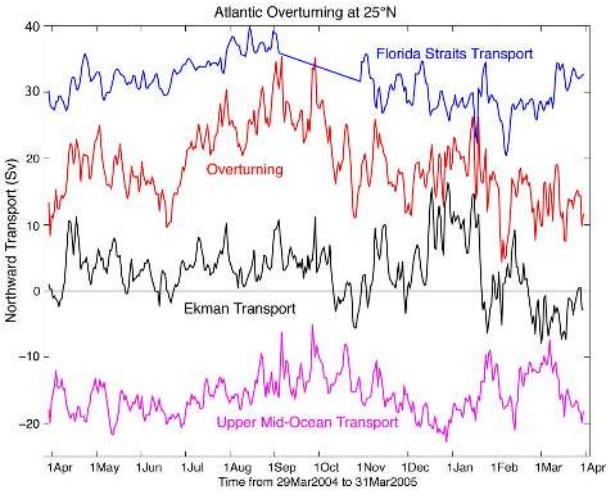

Fig. 2. Daily time series of Florida Straits transport (blue), Ekman transport (black), upper mid-ocean geostrophic transport (magenta) and overturning transport (red) for the period 29 March 2004 to 31 March 2005. Florida Straits transport is based on electromagnetic cable measurements. Ekman transport is based on QuikScat-determined winds. The geostrophic transport is based on Rapid time series of dynamic height at the eastern and western boundaries of the 25° N section and the reference level velocity is set by forcing the geostrophic transport to equal the Florida straits plus Ekman transport on a daily basis. Upper mid-ocean transport is the vertical integral of the transport per unit depth down to the deepest northward velocity (approximately 1100 m depth) on each day. Overturning transport is then the sum of the Florida Straits, Ekman and upper mid-ocean geostrophic transports and represents the maximum northward transport of upper layer waters on each day.

steady Trade Winds so that we can monitor the northward surface Ekman transport with standard wind products. Finally, at 26.5° N there have been measurements of the structure and transport of the Antilles Current and of the deep western boundary current over 12 years from 1985 to 1997 (Bryden et al., 2005) that allow us to design the Rapid array to cost effectively monitor the boundary currents.

In addition to the ongoing Gulf Stream and Ekman transport measurements, the key elements of the Rapid array to monitor the mid-ocean meridional flow components are time series dynamic height profiles over the full water column near the eastern and western boundaries and co-located bottom pressure time series. The Rapid array was first deployed in February–March 2004. The first year of boundary mooring observations has been used to monitor the temporal variability in mid-ocean layer transports (Fig. 1) and the southward mid-ocean thermocline transport has been combined with northward Gulf Stream and Ekman transports to produce a time series of the Atlantic meridional overturning circulation (Fig. 2, Cunningham et al., 2007). Kanzow et al. (2007) demonstrated that the Rapid array measurements satisfy mass conservation for time scales longer than 10 days, proving that the array is effectively monitoring the basin-scale circulation. Here we look more closely at the internal dynamics of the circulation to examine the temporal adjustments that lead to mass conservation. How does the mid-ocean interior circulation adjust to changes in Gulf Stream flow through Florida Straits and in Ekman layer flow? What happens when the deep western boundary current stops? Are baroclinic and barotropic components independent?

We use the same components as Cunningham et al. (2007) except that here we will examine dynamic height profiles and bottom pressure separately for the western and eastern boundaries, as well as at tall moorings wb3 and wb5 near the western boundary, to examine the structure of the temporal changes in baroclinic and barotropic components. We will also examine how dynamic height and bottom pressure relate to sea surface height variations measured by satellites.

2 Methods

For dynamic height, instruments measuring temperature, conductivity and pressure are distributed over depth on a set of moorings along 26.5° N (Fig. 3). Before and after each mooring deployment and recovery, each instrument is put on the CTD package and lowered to the bottom in order to calibrate the moored instrument time series to the high quality pre- and post-CTD profiles, as described by Cunningham et al. (2006). The calibrated time series measurements at 20 min intervals over the year's deployment are then low-pass filtered to remove tides, inertial oscillations, etc. to yield 12 hourly values and then pressure, temperature

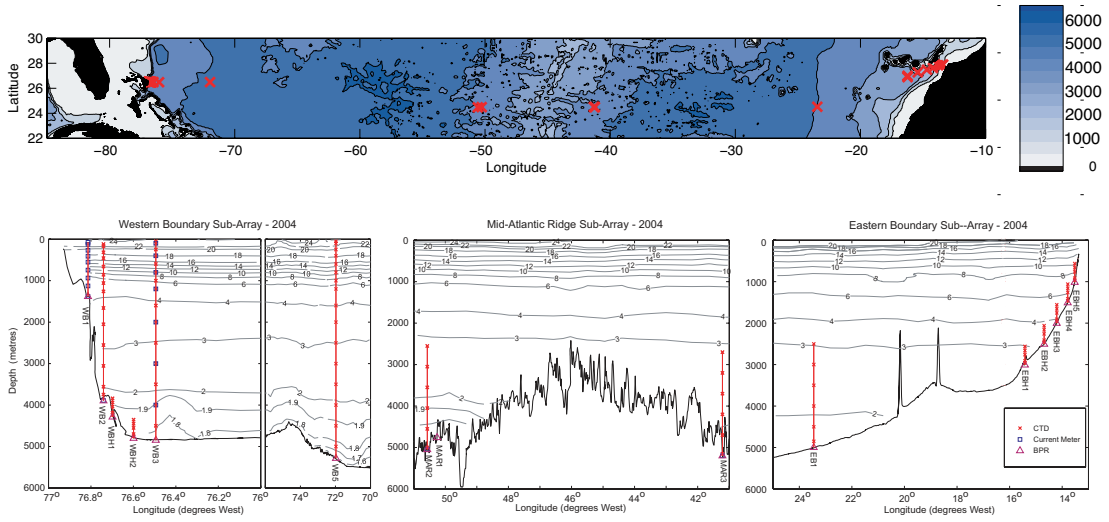

Fig. 3. Rapid array along 26.5° N during 2004–2005: **(a)** location in latitude and longitude of each mooring; **(b)** location of instruments versus depth and longitude along 26.5° N. Only instruments that returned year-long time series are shown. Principal components are 15 bottom pressure records and 12 dynamic height moorings concentrated near the western and eastern boundaries.

and salinity are used to calculate specific volume anomaly time series that are then integrated vertically to produce dynamic height profiles at each mooring site. Cunningham et al. (2007) described how the dynamic height profile from the surface to 4820 dbar at the western boundary is created by joining measurements on wb2, wbh1 and wbh2 and how the dynamic height profile at the eastern boundary from the surface to 5200 dbar is created by joining measurements on moorings eb1, ebh2, ebh3, ebh4 and ebh5 crawling up the continental slope. We will refer to these western and eastern boundary profiles as dynamic height at wb2 and ebh. Similarly, dynamic height profiles are created for the tall wb3 and wb5 moorings 50 km and 500 km east from the western boundary. For each site (wb2, wb3, wb5 and ebh), we then create a temporal mean dynamic height profile over the period March 2004 to April 2005. The difference between the mean eastern and western dynamic height profiles, when divided by the Coriolis parameter and vertically integrated, is equal to the mean geostrophic mid-ocean meridional transport. This geostrophic mid-ocean transport must balance the mean Gulf Stream plus Ekman transport and this constraint effectively sets the mean reference level velocity (and mean bottom pressure difference), as described by Cunningham et al. (2007). Here, we examine the 12 h anomalies in dynamic height with respect to the mean profiles at each site.

For bottom pressure, the 2004–2005 Rapid array included 15 bottom pressure gauges: from west to east, they were at the following moorings (Fig. 3):

wb1, wb2, wbh1, wbh2, wb3, wb5, mar2, mar1, mar3, eb1, ebh1, ebh2, ebh3, ebh4, and ebh5.

wb1 and ebh5 are very shallow; wbh2 is not consistent with surrounding records on wb2, wbh1 and wb3; mar1 suffers from mooring motion as it floated slightly above the bottom; and ebh1 appears to have a jump in mid record. Thus, we concentrate here on 10 deep bottom pressure records across the width of the North Atlantic at about 26.5° N:

wb2, wbh1, wb3, wb5, mar2, mar3, eb1, ebh2, ebh3, and ebh4.

Four are near the western boundary, two on the Mid Atlantic Ridge, and four near the eastern boundary, so there is a relatively even distribution across the Atlantic but with four near the eastern and four near the western boundaries. Each record consists of 20 min time series of pressure and temperature. Each record is low-pass filtered to remove semi-diurnal and diurnal tides, and an exponential trend is removed to account for drift in each pressure sensor (Fig. 4; Kanzow, 2006). In addition, each record has been analysed to estimate M_f and M_m 14-day and 28-day tidal constituents and these components have been subtracted out of the pressure records. Finally, since the exact depth of each pressure gauge is not known, the record-length average pressure is removed for each pressure gauge and we examine here the 12 h anomaly in bottom pressure for each site.

Gulf Stream transport is obtained on a daily basis from the Florida Straits cable time series (www.aoml.noaa.gov/phod/floridacurrent). Ekman transport is estimated on a daily basis by dividing QuikScat zonal wind stress values (http://winds.jpl.nasa.gov/missions/quikscat/index.cfm) by the surface density and by the Coriolis parameter f and integrating zonally across the basin at 26° N.

To examine relations between dynamic height, bottom pressure, sea surface height, Gulf Stream and Ekman transports, we calculate correlation coefficients versus time lag. In general maximum correlation occurs with zero time lag,

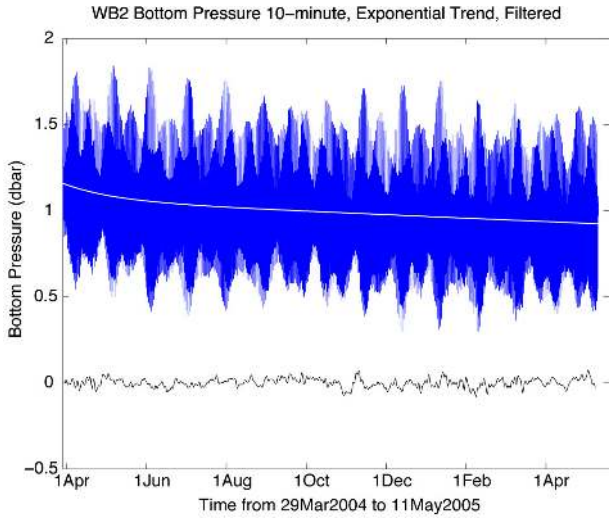

Fig. 4. Bottom pressure record at mooring wb2. 20 min values exhibit strong tidal oscillations and a clear exponential drift with time is also apparent due to sensor creep (upper curves offset by 1 dbar). After tidal filtering and removing the exponential drift, the low-passed 12 hourly time series of bottom pressure (lower curve, mean removed) reveals an rms amplitude of 0.022 dbar.

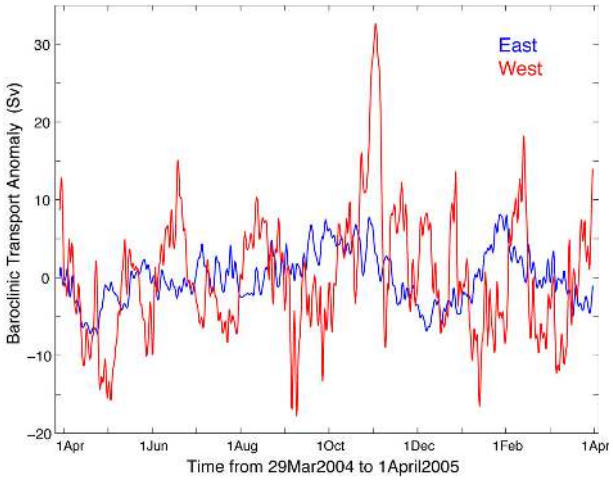

Fig. 5. Baroclinic transport variability near the western and eastern boundaries. Dynamic height anomaly profiles are vertically integrated on a daily basis and divided by the Coriolis parameter to yield baroclinic transport variability in Sverdrups. Dynamic height at the west is made up from temperature-salinity-pressure time series on moorings wb2, wbh1 and wbh2 and at the east from time series on moorings eb1, ebh1, ebh2, ebh3 ebh4, as described by Cunningham et al. (2007).

unless reported otherwise. Cunningham et al. (2007) have estimated the integral time scales for temporal variability in the time series used here to be 24 days. For the 366 day time series, there are then 15 independent time periods, or 13 degrees of freedom, from which we determine that correlations greater than 0.514 are significantly different from zero at a 95% confidence level. We therefore concentrate discussion in the text on correlations greater than 0.51.

3 Analysis

3.1 Baroclinic variability

We first assess the contributions to variability resulting from temperature and salinity anomalies at the western and eastern boundaries; we will call this baroclinic variability. Dynamic height anomaly profiles divided by Coriolis parameter yield geostrophic velocity anomaly profiles that can be integrated vertically to yield local transport variability following the methodology described by Longworth (2007). First we integrate the dynamic height anomalies from bottom to surface to estimate the total west (wb2) and east (ebh) baroclinic transport variability (Fig. 5). The variance in the west is a factor of five larger than that at the east with standard deviations in western and eastern baroclinic transport of 7.9 Sv and 3.3 Sv respectively. We can also do the vertical integration over layers and we choose the same depth intervals used by Cunningham et al. (2007) to estimate the transport variability in the thermocline recirculation (0 to 800 m depth), intermediate water (800 to 1100 m), upper North Atlantic Deep Water (UNADW, 1100 to 3000 m) and lower North Atlantic Deep Water (LNADW, below 3000 m) for the western (wb2) and eastern (ebh) sites (Table 1). The transport variability in the thermocline recirculation (0 to 800 m depth) is only slightly larger in the west than in the east; but variability in deep water transports is much greater in the west as there is very little deep transport variability in the east at ebh. Thus, as found also by Longworth (2007) in an analysis of historical hydrographic stations, baroclinic variability near the western boundary is much larger than that at the eastern boundary.

3.2 Bottom pressure

For bottom pressure, the first notable feature of the 10 bottom pressure records is that the pressure goes up and down in unison for all 10 pressure gauges (Fig. 6a). The standard deviation (equal to the root mean square value or rms) of the 12 hourly zonal average (over 10 records) pressure is 0.0150 dbar. All across the ocean at 26.5° N, bottom pressure rises and falls on about a 5 to 10 day time scale with an rms amplitude equivalent to an rms rise and fall in sea level of about 1.5 cm. The entire Atlantic Ocean at 26° N appears to be filling and draining (see Appendix A for a brief analysis of the origins of the zonally averaged pressure fluctuations). To remove this signal so as to avoid contaminating local bottom pressure fluctuations with the strong fluctuations in zonally averaged bottom pressure, we subtract the zonal average pressure (Fig. 6b, a straight average of the 10 bottom pressure records) from each individual record at each 12 h interval. The resulting rms pressure signal is reduced from about

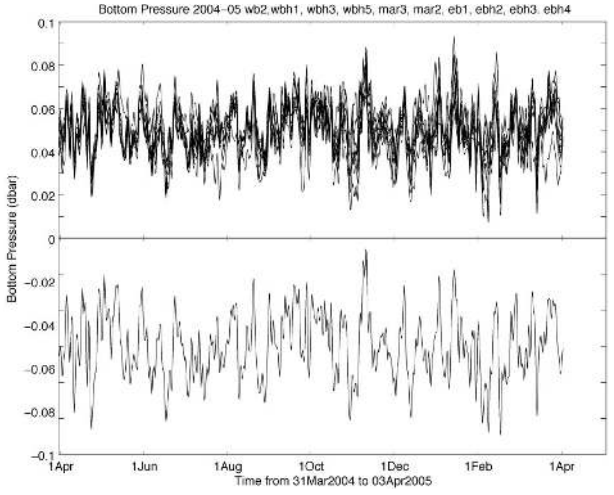

Fig. 6. Bottom pressure time series: **(a)** at 10 sites across the Atlantic at 26.5° N (each offset by 0.08 dbar) and **(b)** the zonal average bottom pressure on each day (offset by −0.05 dbar). Note that bottom pressure appears to rise and fall in phase at all 10 sites.

0.019 dbar to about 0.012 dbar, a 60% reduction in variance (Table 2). To put the values in context, a 0.02 dbar bottom pressure signal, if it is depth independent over 5000 m depth and in geostrophic balance and unmatched by the same signal on the other side of the basin, would represent a geostrophic transport signal of 15 Sv. Clearly, however, to first order the high frequency bottom pressure fluctuations on the west and on the east have similar amplitude so their difference which is proportional to a barotropic transport is much smaller than their individual amplitudes. Again the variance in bottom pressure is larger at the west than at the east, but only slightly larger (excluding the wb5 record that looks somewhat anomalous).

3.3 Baroclinic-barotropic compensation

Baroclinic transport anomalies arise due to changes in temperature and salinity. Right at the western boundary, they are perhaps due to Rossby waves or eddies propagating westward and hitting the boundary or perhaps due to Kelvin waves propagating southward along the continental slope. At the eastern boundary the anomalies may be due to changes in the upwelling regime or to Kelvin waves propagating northward along the continental slope. In the calculations by Cunningham et al. (2007) that assumed mass compensation, a baroclinic transport anomaly is compensated by a depth-independent or barotropic adjustment in the basin-scale flow. We might hypothesise a local barotropic adjustment to a baroclinic transport anomaly whereby the bottom pressure changes each day at the base of the mooring so that the vertical integral of the bottom pressure anomaly (bottom pressure anomaly times 4800 m depth) exactly cancels the baroclinic transport anomaly observed on the mooring that day. The resulting pressure profile (dynamic height profile relative to the bottom + predicted bottom pressure) then has zero vertical integral, and the total transport anomaly is zero. Thus, locally we can predict a compensating bottom pressure anomaly for each day so that the overall local transport anomaly (barotropic + baroclinic transport) is zero.

Remarkably, at the western boundary at wb2 this predicted bottom pressure anomaly is strongly correlated with the observed bottom pressure time series after subtracting out the zonally uniform signal (Fig. 7): observed and predicted bottom pressures at wb2 have similar amplitude, no apparent phase shift and a significant correlation of 0.62. Thus, the bottom pressure at the western boundary appears to be

Table 1. Baroclinic Transport Standard Deviation (Sv). Transports are vertically integrated dynamic height anomaly divided by f.

	East	West
Overall	3.32	7.89
0–800 m	2.43	2.97
800–1100 m	0.49	0.87
1100–3000 m	0.70	4.22
Below 3000 m	0.08	0.77

Table 2. Bottom Pressure Variability. Each pressure record has had an exponential drift removed, each has been low-pass filtered to remove high frequency tidal and intertial oscillations, and each has been fitted to remove fortnightly M_f and monthly M_m tidal components. The resulting bottom pressure variations exhibit standard deviations ranging from 0.016 to 0.026 dbar. All records exhibit synchronous rise and fall of pressure on a 5 to 10 day time scale. Thus we estimate a zonally averaged bottom pressure over the 10 records (Fig. 4b) and remove it from each bottom pressure record. The zonally averaged bottom pressure has a standard deviation of 0.0150 dbar. After removing the zonally avearged pressure, the resulting bottom pressure records exhibit standard deviations ranging from 0.009 to 0.022 dbar, a 60% reduction in variance.

	Mooring std dev (dbar)	Individual-Average std dev (dbar)
wb2	0.0218	0.0118
wbh1	0.0226	0.0131
wb3	0.0210	0.0109
wb5	0.0261	0.0215
mar2	0.0173	0.0105
mar3	0.0168	0.0100
eb1	0.0189	0.0146
ebh2	0.0157	0.0094
ebh3	0.0165	0.0102
ebh4	0.0165	0.0095

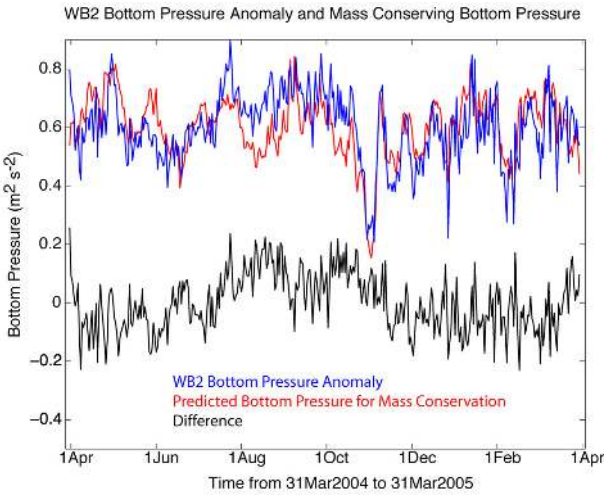

Fig. 7. Bottom pressure at wb2. The bottom pressure anomaly (blue) is defined to be the bottom pressure measured at wb2 minus the zonal average bottom pressure shown in Fig. 6b. Predicted bottom pressure (red) is that required to compensate for local baroclinic transport variability shown in Fig. 5. The difference between bottom pressure anomaly and predicted bottom pressure at wb2 is shown in black. The blue and red curves have been offset from the black curve by adding 0.06 dbar to them.

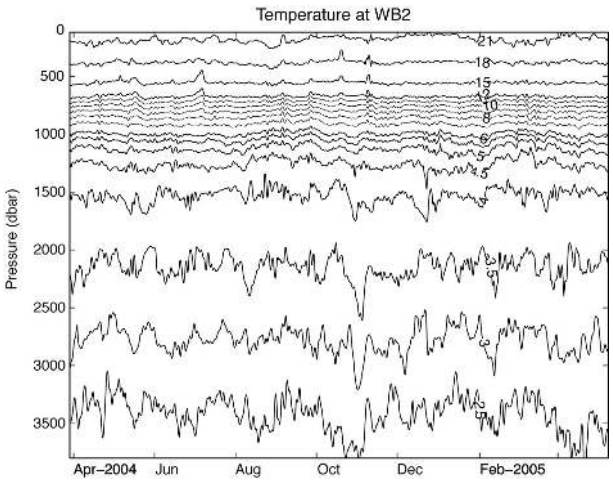

Fig. 8. Contoured time series of temperature profiles measured on wb2 at the western boundary. Note the steep descent of deep isotherms in early November 2004 that marks the shutdown in the southward flow of lower North Atlantic Deep water.

responding to local changes in baroclinic transport due to fluctuations in temperature and salinity and compensating for variations in baroclinic transport.

To describe this baroclinic transport compensation mechanism with an example, we examine the event in early November 2004 that is the largest event in both baroclinic transport anomaly and bottom pressure anomaly. In early November, deep temperatures at the western boundary (wb2) warmed substantially with isotherms deepening by about 700 m (Fig. 8). Such anomalous warming leads to positive dynamic height anomaly as indicated in Fig. 9 (blue) leading to a mid-ocean southward transport anomaly if the eastern boundary dynamic height anomaly remains constant. For this event the transport anomaly is more than 30 Sv (Fig. 5). The predicted bottom pressure anomaly to compensate the transport anomaly is a negative offset whose vertical integral balances the vertically integrated dynamic height. Remarkably, the observed bottom pressure anomaly at wb2 is almost exactly equal to the predicted compensation pressure as shown in Fig. 7. The resulting dynamic pressure anomaly profile, bottom pressure + dynamic height (Fig. 9, green) is then subtracted from the mean transport per unit depth profile (Fig. 9, black) to produce the mid-ocean transport per unit depth profile (Fig. 9, red) that shows that the southward transport of lower North Atlantic Deep water (LNADW) below 3000 m effectively stopped during this event. From associated direct measurements during this event, Johns et al. (2008) also observed the stoppage in the southward flow of LNADW.

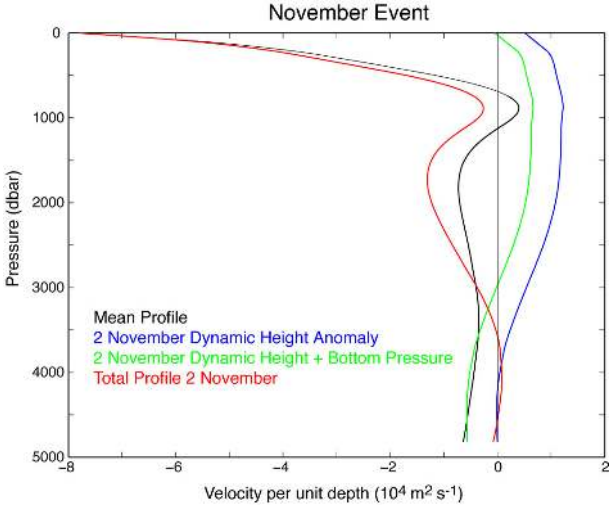

Fig. 9. Vertical profiles of transport per unit depth during the November 2004 event at wb2. The mean mid-ocean transport per unit depth profile (black line) is derived from the difference between time-averaged dynamic height profile2 at ebh and wb2. The dynamic height anomaly profile for the November event at wb2 (blue line) reflects the presence of warmer deep waters at the western boundary as seen in Fig. 8. The dynamic height profile + the observed bottom pressure anomaly at wb2 (green line) represents the total anomaly profile for the November event at the western boundary. The final mid-ocean transport per unit depth profile for the November event (red line) is the difference between the mean profile and the anomaly profile and assumes zero anomaly at the eastern boundary. Note the shutdown in the southward flow of lower North Atlantic Deep water below 3000 m depth with an actual reversal to northward flow below 3500 m depth.

For the eastern boundary and for moorings wb3 and wb5, there is also a partial local compensation of baroclinic transport variability by bottom pressure changes, but the compensation is not as strong as for wb2. Correlations between locally predicted and measured bottom pressure are only 0.09 for wb3, 0.38 for wb5 and 0.42 for ebh. Whilst there is some evidence for local compensation at each site, none of the correlations for wb3, wb5 and ebh is statistically significant. Only the site wb2 right at the western boundary appears to be especially constrained for the barotropic transport variations due to bottom pressure to match (and cancel) the baroclinic transport variations due to dynamic height anomalies at the boundary. At the western boundary, baroclinic and barotropic (bottom pressure) fluctuations are not independent; baroclinic and barotropic fluctuations at the western boundary co-vary so as to reduce the basin-scale transport variations.

3.4 Vertical structure

Adding local daily bottom pressure anomaly to the dynamic height anomaly profile at each of wb2, wb3, wb5 and ebh yields time series of geostrophic pressure profiles for which we can estimate empirical orthogonal functions (eof's) for the vertical structure in geostrophic pressure (equivalent to a profile of northward transport per unit depth when geostrophic pressure is divided by the Coriolis parameter). At wb2 (Fig. 10), the first mode accounting for 56% of the variance is surface intensified, exhibits the same sign from surface to bottom but has a modulation from 1000 to 4000 dbar that may reflect the 2-lobed structure of the deep western boundary current. The second mode, accounting for 23% of the variance, looks like a classical first baroclinic mode with a surface pressure of opposite sign to the bottom pressure. The third mode looks like a classical second baroclinic mode and accounts for 14% of the variance. Away from the western boundary, the first eof for wb3, wb5 and ebh has the same sign from top to bottom and exhibits a surface intensified structure above 1000 dbar and relatively depth-independent structure below 1000 dbar, a structure that is often described as a coupled barotropic – baroclinic mode (Fig. 11). The second eof in each case looks like a first baroclinic mode. The first eof's account for 71%, 61% and 61% and the second eof's account for 18%, 31% and 37% of the variance at wb3, wb5 and ebh, respectively.

Correlation coefficients between the geostrophic pressure (dynamic height relative to the bottom plus bottom pressure) at 100 dbar and bottom pressure are relatively small: -0.14 for wb2, 0.20 for wb3, 0.16 for wb5 and -0.23 for ebh. The reason for low correlation can be partially understood in terms of these vertical modes: the first mode with about 60% of the variance exhibits positive correlation between near-surface geostrophic pressure and bottom pressure but the second mode with about 25% of the variance contributes negative correlation, partially cancelling out the positive correlation from the first mode. In addition, the bottom pressure fluctuations are much smaller than the near surface geostrophic pressure fluctuations. We expect surface geostrophic pressure to closely match sea surface height variability. Thus, on the basis of these 4 moorings combining dynamic height and bottom pressure, we would not expect to observe a correlation between sea surface height and bottom pressure. The vertical structure appears to consist of a coupled barotropic-baroclinic mode, that Chelton et al. (2007) call an eddy-like structure, and a first baroclinic mode, often referred to as a baroclinic Rossby wave. The coupled barotropic-baroclinic mode dominates by roughly 2 to 1, but not enough that there is a consistent correlation between surface geostrophic pressure and bottom pressure.

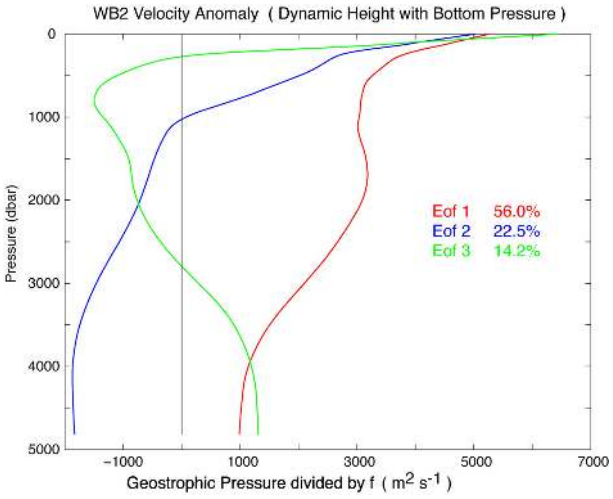

Fig. 10. Empirical orthogonal functions for the vertical structure in geostrophic pressure divided by f at wb2. Bottom pressure anomaly (difference between measured bottom pressure and zonally averaged bottom pressure) is added to the dynamic height anomaly profile at each day to estimate geostrophic pressure which is then divided by the Coriolis parameter to generate a profile of transport per unit depth in $m^2\ s^{-2}$. The first 3 eof's illustrate the vertical structure in the daily time series.

3.5 Sea surface height

Altimetric measurements of sea surface height (ssh) have been regularly made since the launch of the Topex-Poseidon satellite in 1992. Comparison of ssh from the DUACS (Developing Use of Altimetry for Climate Studies) merged altimeter data from the ERS (European Remote Sensing), TOPEX/Poseidon, Envisat, and Jason satellites are interpolated from the standard grid ($1/3° \times 1/3°$) at 7-day intervals to the positions of wb2, wb3 and wb5 with dynamic height anomalies from the mooring data (Fig. 12) exhibit reasonable agreement between dynamic height and ssh variability with correlation coefficients of about 0.8. There is more high frequency content in the dynamic height daily time series

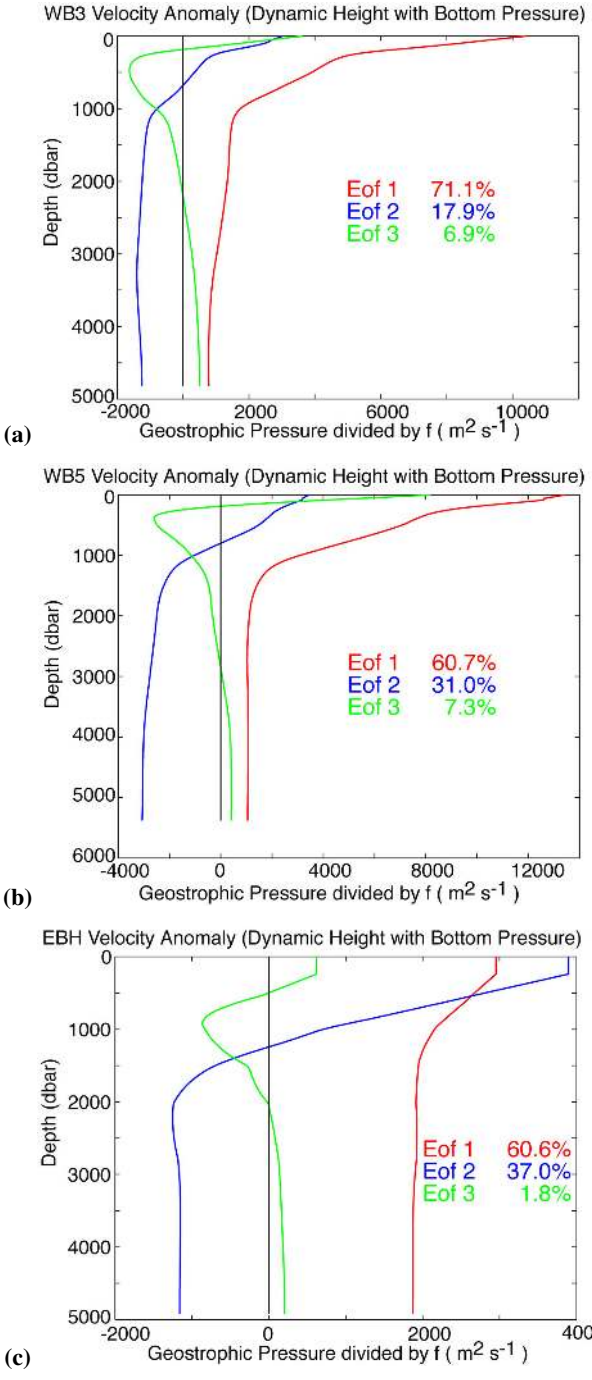

Fig. 11. Empirical orthogonal functions for the vertical structure in geostrophic pressure divided by f at moorings wb3 **(a)**, wb5 **(b)** and ebh **(c)**.

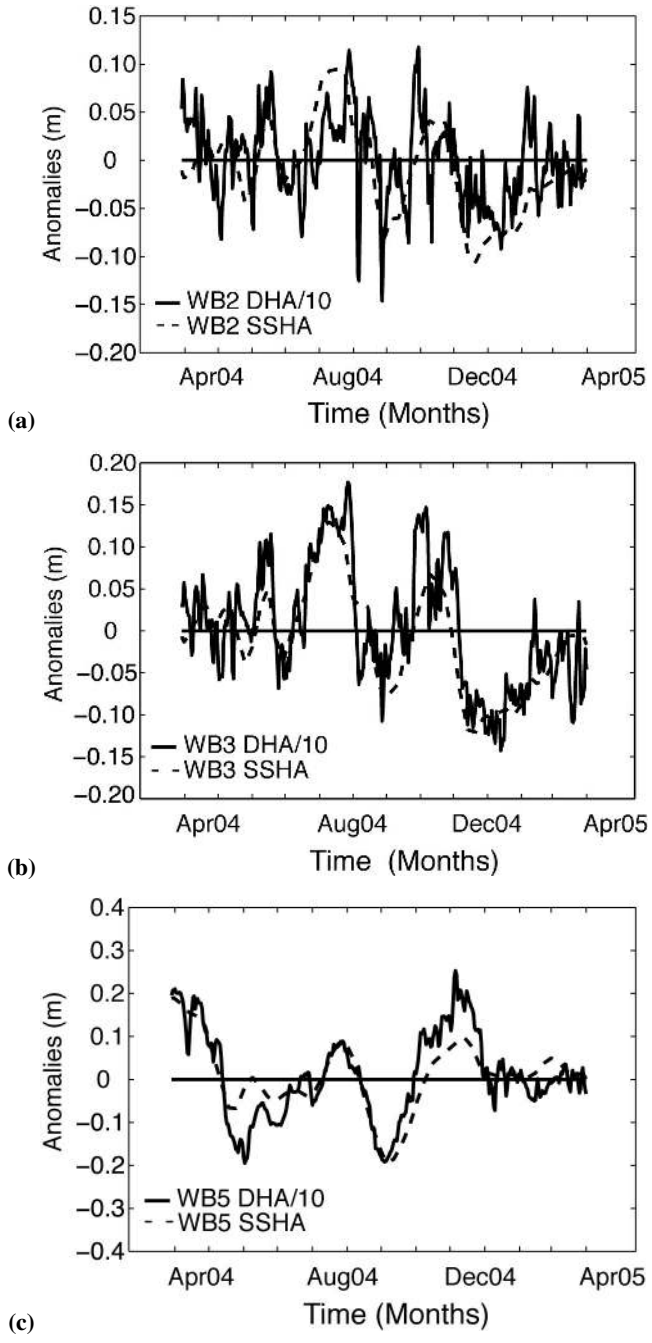

Fig. 12. Temporal variability in sea surface height (ssh) and dynamic height at the sea surface at moorings wb2 **(a)**, wb3 **(b)** and wb5 **(c)**. Sea surface height in centimetres is from DUACS (Developing Use of Altimetry for Climate Studies) merged altimeter data from the ERS (European Remote Sensing), TOPEX/Poseidon, Envisat, and Jason satellites. The DUACS handbook has further details and can be found at http://www.jason.oceanobs.com. At each time, the gridded DUACS ssh values are linearly interpolated in space onto the position of the moorings. Dynamic height at the sea surface is in dyn cm (0.1 $m^2\ s^{-2}$).

of course; there is an offset in time between events at the 3 mooring sites of up to 2 days that likely results from the time within the 7 day interval of the nearest satellite ground-track; but the amplitudes of ssh and dynamic height anomaly are similar (Table 3).

Table 3. Standard Deviation of Sea Surface Height (ssh) and Dynamic Height. The ssh values are for the time period 29 March 2004 to 31 March 2005 to match the time period of the dynamic height variations. The ssh values in parentheses are for the 13 year time period 1992–2005. 100 dbar is typically the shallowest instrument depth in the Rapid array so dynamic height at the surface is an extrapolation of the dynamic height anomaly from 100 dbar to the surface.

Site	ssh (cm)	dynamic height (100 dbar) (dynamic cm)	dynamic height (0 dbar) (dynamic cm)
wb2	4.83 (5.50)	3.46	4.66
wb3	6.22 (6.78)	5.40	7.24
wb5	7.66 (9.66)	8.64	10.57

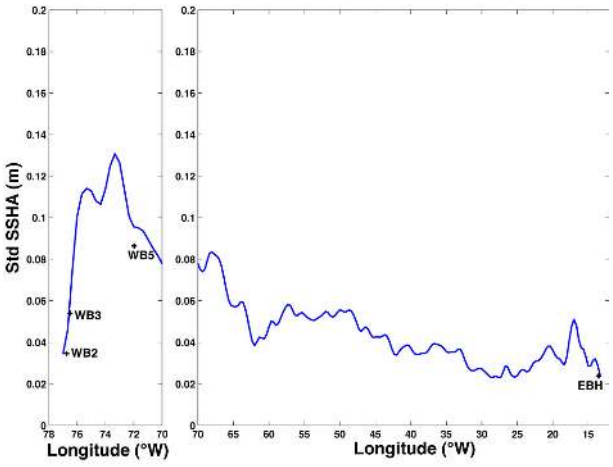

Fig. 13. Standard deviation in sea surface height variability (cm) versus longitude at 26.5° N. The continuous curve is from DUACS (Developing Use of Altimetry for Climate Studies) merged altimeter data from the ERS (European Remote Sensing), TOPEX/Poseidon, Envisat, and Jason satellites. The standard deviation in dynamic height at moorings wb2, wb3, wb5 and ebh are indicated by crosses at the appropriate longitudes. The horizontal scale is expanded west of 70° W to show the sharp drop in ssh (and dynamic height) variability as the western boundary is approached.

It is notable that both ssh and dynamic height show a decrease in variance toward the boundary (Fig. 13). On its own, the striking decrease in the variance in ssh as land is approached might have reasonably been considered to be the result of boundary effects in the satellite altimetric measurements. However, the dynamic height time series also show a striking decrease in variance with the standard deviation in 100 dbar dynamic height decreasing from 8.6 dynamic centimetres at wb5, 500 km from the boundary, to 5.4 at wb3 50 km from the shore, to 3.5 at wb2 23 km from Abaco. Remarkably, the western boundary appears to exert a strong constraint on the size of variability in ssh and dynamic height relative to offshore variability. Kanzow et al. (2009) provide dynamical arguments for how eddies interact with the western boundary leading to this sharp decrease in eddy amplitude close to the boundary.

3.6 Gulf Stream and Ekman transport compensation

It is of interest to know how the fluctuations in Gulf Stream transport are balanced by the mid-ocean flow. Cunningham et al. (2007) already reported that the Gulf Stream, Ekman and mid-ocean thermocline components of the overturning are not significantly correlated, so we concentrate here on compensation by bottom pressure fluctuations. We first removed the predicted bottom pressure based on baroclinic transport variations from the observed bottom pressure at wb2 in order to examine how this reduced pressure anomaly relates to the Gulf Stream transport through Florida Straits. We multiply the reduced bottom pressure at wb2 by 4000 m depth and divide by the Coriolis parameter to derive a time series of geostrophic mid-ocean transport due to fluctuations at wb2. The baroclinic transport anomaly has already been compensated by the predicted part of the bottom pressure that we removed. Thus, the reduced pressure anomaly represents the residual geostrophic transport that is effectively barotropic. The resulting geostrophic mid-ocean transport time series is correlated to the fluctuations in Gulf Stream transport through Florida Straits: for daily values the correlation is 0.51 and for 10-day low-passed values the correlation is 0.61. The sign of the correlation is notable: higher Gulf Stream transport is correlated with higher bottom pressure at the western boundary at wb2 which indicates southward barotropic geostrophic transport in the interior basin at 26° N. The correlation falls rapidly, at wb3 50 km east of the Bahamas the correlation has dropped to 0.34 and by wb5 the correlation has effectively vanished. The geostrophic transport associated with the bottom pressure anomaly at the western boundary is noisy but a scatter plot (Fig. 14) shows a clear relationship between reduced bottom pressure anomalies and Gulf Stream transport fluctuations. Arguably, the amplitude of the reduced bottom pressure is even correct, remarkable in that we just chose 4000 m as the depth over which to apply the barotropic transport; choosing 4230 m for the depth scale would have led to the barotropic transport variations having the same rms amplitude as the Gulf Stream transport variations.

We were unable to increase the correlation between Gulf Stream transport and bottom pressure fluctuations, for example by using the difference between wb2 and wb3 or between wb2 and eb1. Thus, fluctuations in the Gulf Stream transport through Florida Straits appear to be balanced by a compensating change in bottom pressure right at the western boundary of the mid-ocean section. The compensation appears to be instantaneous though we admit that the remnant bottom

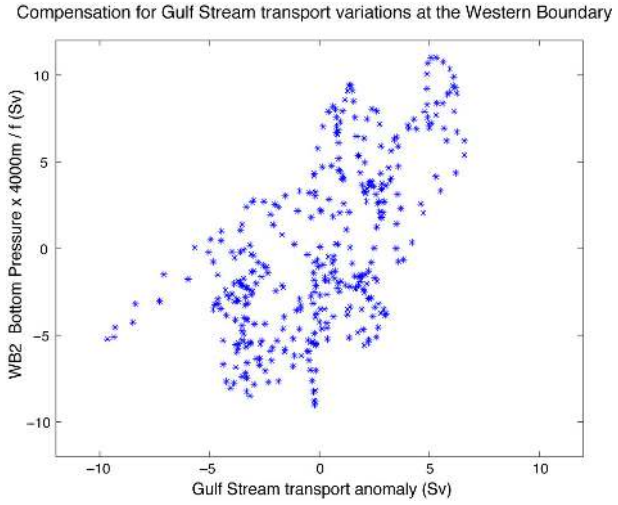

Fig. 14. Scatter plot of bottom pressure at wb2 and Gulf Stream transport anomaly (Sv). The bottom pressure is the difference between bottom pressure anomaly at wb2 and the predicted bottom pressure required to compensate for baroclinic transport variations at wb2 (as described in Fig. 7). This bottom pressure is then multiplied by a scale depth of 4000 m and divided by f to convert it into a western boundary transport anomaly in Sv. Both bottom pressure and Gulf Stream transport time series have been low-passed filtered with a cut-off at 10-day period. The correlation coefficient for the two time series is 0.62.

pressure time series remains quite noisy after removing the tides, an exponential drift, a fluctuating basin-scale average bottom pressure and a bottom pressure component that compensates for baroclinic transport variations at wb2.

For fluctuations in Ekman transport, we first examined correlations between Ekman transport and bottom pressure records at wb2, wbh1, wb3, wb5, wb2, wbh1, wb3, wb5, mar3, mar2, eb1, ebh2, ebh3, ebh4 and found highest correlations at wbh1 (0.41) and eb1 (−0.44). Taking the difference wbh1–eb1 led to an even higher correlation of 0.47 and for 10-day low-passed series the correlation increased to 0.57. An eof analysis for the zonal structure in bottom pressure yields a first mode with high pressure near the western boundary and low pressure in the eastern boundary accounting for 46% of the variance. The first mode time series is also correlated with Ekman transport variability at 0.36. Thus, variations in Ekman transport appear to be compensated by a bottom pressure difference that spans the ocean basin from the western boundary at wbh1 to the eastern boundary at eb1. We rationalise the small correlation (0.11) between Ekman transport and wb2 bottom pressure as being due to the signal at wb2 being masked by the larger baroclinic and Gulf Stream compensations at wb2. More troubling is that the bottom pressure difference fluctuations (when turned into transport by multiplying by 4000 m depth and dividing by f) appear to be a factor of 3 larger than the variations in Ekman transport. Thus, although there is good correlation between basin-scale bottom pressure difference and Ekman transport, the magnitude of the barotropic flow derived from the bottom pressure difference is much larger than the Ekman transport and as a result we feel we do not yet understand how the variations in Ekman transport are compensated in the basin-scale circulation.

4 Discussion

The variability in the meridional overturning circulation at 26° N reported by Cunningham et al. (2007) is smaller than anticipated. Based on satellite altimetric estimates of sea surface height variability associated with eddies, Wunsch (2008) has recently argued that the rms variability in overturning should be 16 Sv. In sharp contrast, Cunningham et al. (2007) estimated variability in the upper mid-ocean transport of only 3.3 Sv. On the basis of the analysis here, the smallness of the observed variability in the overturning at 26° N has two causes: first, eddy variability reduces sharply as the western boundary is approached; and secondly, there is strong compensation between components of the overturning so that the overall variability in overturning is much smaller than the variability in individual components.

Eddy variability in both upper ocean dynamic height and sea surface height (ssh) decreases markedly westward along 26° N as the western boundary of the Bahamas is approached (Fig. 11). When we first plotted ssh variability from satellite altimeters versus longitude, colleagues said that the reduction in variability near the western boundary was due to land effects in the satellite measurements. But the dynamic height time series from the moorings show agreement in amplitude and timing with the satellite ssh time series and the dynamic height variance also decreases toward the boundary. Thus the evidence is compelling that variability in sea surface height indeed decreases toward the western boundary. Our initial qualitative argument was that eddies generate most of the upper ocean variability in ssh and that the centre of a circular eddy could not make it to the coastline because the flow of the eddy toward the boundary would quickly move away along the boundary so the eddy would decay as it approached the boundary. Kanzow et al. (2009) have now put such a qualitative argument into a dynamical framework to show how eddies or waves dissipate as they approach the western boundary.

In terms of compensating components, Kanzow et al. (2007) showed a remarkable compensation between what they called the internal and external modes of variability. Here we find that the baroclinic transport (internal mode) variability at the western boundary with an rms value of 7.9 Sv (Table 1) is compensated locally and instantaneously by variability in bottom pressure (external mode) that effectively cancels the depth-integrated baroclinic transport variability (Fig. 7). There is still variability in upper (or lower)

layer transport, but due to the local compensation such variability is reduced to about 3 Sv. This compensation mechanism is especially effective in cancelling out the variability in deep water transports as dramatically observed for the November event (Fig. 9). There, the baroclinic transport anomaly of more than 30 Sv is concentrated in the deep water of the western boundary current; the compensation by the observed bottom pressure is depth-independent so it nearly cancels the deep transport anomaly that occupies much of the water column, leaving only a small anomaly in the overturning defined to be either the upper (shallower than 1000 dbar) or lower (deeper than 1000 dbar) transport. What might be considered to be a 30 Sv anomaly in overturning if components are considered individually turns out to be an unremarkable anomaly in overturning of less than 3 Sv.

There is also compensation for Gulf Stream transport variations by the bottom pressure variations just east of the Bahamas, but this mechanism is not so effective at reducing the variability in the overturning. The Gulf Stream is a shallow flow above 800 m depth; when it is stronger than average, the bottom pressure anomaly at wb2 increases to compensate, leading to a southward transport that compensates for the stronger northward Gulf Stream flow. Because the compensating transport is depth-independent, only about 20% of the compensation occurs in the upper 800 m to reduce the northward upper ocean transport anomaly associated with the Gulf Stream. Thus about 80% of Gulf Stream transport variations carry through to variations in the overturning, in contrast to the near cancellation of deep baroclinic transport anomalies.

To monitor basin-scale ocean circulation, it is crucial to measure as close to the western boundary as possible. The Rapid monitoring system takes advantage of the steep topography at the western "wall" to deploy a tall deep-water mooring (wb2) less than 23 km from the shoreline. Instrumented with temperature, salinity, pressure recorders throughout the water column and with a bottom pressure recorder, this tall mooring provides time series profiles of geostrophic pressure close to the boundary. Inshore (west) of this mooring, the Rapid array is designed to measure current velocities directly in the boundary wedge. At the outset, the Rapid array design aimed to put this mooring as close to the boundary as possible to reduce the area of the boundary wedge requiring direct current measurements. But the closeness has become even more important as a result of the observed reduction in variability as the boundary is approached. The variance in dynamic height at wb2 site is a factor of 6 smaller than at the open ocean site (wb5) 500 km from the boundary and a factor of 2 smaller than at wb3 only 50 km from the western boundary. Thus variability reduces as the western boundary is approached and measuring as close to the boundary as possible improves the ability to measure the signal of basin scale baroclinic transport variability above the level of eddy noise.

Bottom pressure measurements are extremely sensitive with a precision of about 0.001 dbar (Kanzow et al., 2006), but the observed variability in bottom pressure is much larger amounting to 1 dbar or more. To observe subtle dynamical effects in the variability of the large-scale basin-scale ocean circulation, care is needed first to filter out semi-diurnal and diurnal tidal oscillations with amplitude of order 1 dbar, to fit and remove fortnightly and monthly tides and to take account of an exponential drift over time of order 0.25 dbar. But also, we found it necessary to remove a basin-scale fluctuation in pressure of order 0.015 dbar with a time scale of about 5 days before we could examine the compensation mechanisms for baroclinic, Gulf Stream and Ekman transport variability.

The magnitude of the spatially uniform bottom pressure variability surprised us. Fluctuations in sea level with 4 to 6 day periods with large spatial coherence scales have been observed previously in the tropical Pacific and South Atlantic (Luther, 1982; Woodworth et al., 1995) and bottom pressure fluctuations of 4 to 6 day period have been observed with spatial coherence scales of at least 1000 km in the subtropical and tropical North Atlantic (Brown et al., 1975; Kanzow et al., 2005). Still we were surprised by the in phase oscillations in bottom pressure across the 6000 km width of the Atlantic at 26° N (Fig. 6b). Clearly, large spatial scale bottom pressure variability is an important consideration when using local measurements of bottom pressure for dynamical analyses since the zonally uniform pressure component here represented 60% of the low-frequency bottom pressure variability observed locally. We "filtered out" this spatially uniform variability in bottom pressure by taking the zonal average bottom pressure and subtracting it from individual bottom pressure records. But such an approach would not work for analysis of localised bottom pressure records, for example near the western boundary where the spatially uniform component is substantially larger than the dynamically important components that compensate for baroclinic transport variability or for Gulf Stream transport variability. The spatially uniform bottom pressure variability is not related to local atmospheric pressure variability which has larger amplitude and smaller spatial scales. On short time scales it is related to zonally averaged atmospheric pressure but with a phase lag suggesting the North Atlantic Ocean is filling and draining (Appendix A). We urge caution in dynamical interpretations of local bottom pressure observations until the dominant spatially uniform component is identified and, if necessary, removed.

Measuring bottom pressure close to the western boundary is crucial for understanding the origins of variability in the basin-scale overturning. After filtering out high frequency tides and removing the zonally uniform bottom pressure variability, bottom pressure at the western boundary compensates locally for baroclinic transport anomalies resulting from variations in temperature and salinity at the western boundary, particularly those associated with temporal changes in the deep western boundary current. Once the

baroclinic transport compensating pressure is removed from the bottom pressure time series, the residual variability in bottom pressure close to the boundary compensates for Gulf Stream transport anomalies. This Gulf Stream compensating bottom pressure appears to decay quickly eastward from the boundary as it has mostly disappeared at wb3 50 km east of wb2. There may also be a component that compensates for Ekman transport variability but the small errors in estimating the residual bottom pressure fluctuations by subtracting out the tidal, zonally uniform, baroclinic and Gulf Stream components compromises our ability to observe this component at the western boundary site wb2. Thus to understand the mechanisms that balance variations in Gulf Stream transport and deep western boundary current structure, it is essential to measure bottom pressure right at the western boundary.

It is rare to have full-depth moorings measuring temperature and salinity time series throughout the water column with associated bottom pressure measurements so that sea level, atmospheric pressure, geostrophic pressure throughout the water column and bottom pressure can be intercompared and combined to quantify the vertical structure of ocean variability. The Rapid array had 4 tall moorings during 2004–2005: wb2, wb3 and wb5 near the western boundary and ebh near the eastern boundary. For these moorings we find no statistically significant correlation between bottom pressure and sea surface height (defined to be dynamic height referenced to the bottom plus bottom pressure). Empirical orthogonal modes reveal no simple projection onto a consistent vertical modal structure. Only at the westernmost mooring, wb2, is there a significant anti-correlation between vertically integrated dynamic height and bottom pressure fluctuations indicating mass compensation between baroclinic and barotropic fluctuations and suggesting a first baroclinic mode structure with no net vertically integrated flow.

That fluctuations in Gulf Stream and deep western boundary current mass transport are instantaneously compensated by bottom pressure adjustments at the western boundary demonstrates how tight the overall mass conservation constraint is for an ocean basin like the North Atlantic that is nearly closed at its northern boundary. Gulf Stream transport fluctuations, rms of 3.3 Sv, or deep western boundary transport fluctuations, rms of 4.2 Sv, cannot be compensated by equal inflow or outflow through the shallow Bering Straits. Thus, such transport fluctuations quickly lead to changes in sea level height and hence in bottom pressure that can propagate at deep water wave speeds of $\sqrt{gH}$, or 200 m s^{-1} for ocean water depth of 4000 m, to adjust the circulation to balance the initial transport anomaly. Here we find that the Gulf Stream and deep western boundary current fluctuations are compensated by bottom pressure at the western boundary, while Ekman transport fluctuations appear to have a signature in bottom pressure at both the eastern and western boundaries.

Appendix A

After low-pass filtering the individual bottom pressure records to remove high frequency tides, there was a surprisingly large pressure variation common to all individual records that had a standard deviation of 0.0182 dbar representing about 75% of the low frequency variance in bottom pressure. One component of this spatially uniform bottom pressure variability is clearly related to the fortnightly and monthly tidal forcing so we removed these components by fitting and subtracting M_f and M_m signals from individual bottom pressure records. These M_f and M_m components have a standard deviation of 0.0106 dbar and the rms east-west bottom pressure difference for these low frequency tidal fluctuations is 0.0048 dbar, suggesting a north-south geostrophic transport at these tidal frequencies of 3 Sv.

After removing the low frequency tidal components, the zonally averaged bottom pressure had a standard deviation of 0.0150 dbar (Table 2). Much of the variability occurs at periods less than 10 days so we examined the relation between 10-day high-passed zonally avearged bottom pressure, zonally averaged atmospheric pressure and barotropic geostrophic transport (proportional to east minus west bottom pressure difference). For the 4–5 day period, variations in zonally averaged bottom pressure are coherent with zonally averaged atmospheric pressure at 26° N (from NCEP) but there is a 30° phase difference such that bottom pressure peaks 30° before atmospheric pressure. There appears also to be a phase lag where southward geostrophic transport (ebh3–wb2) lags maximum bottom pressure by about 30°. If we combine atmospheric pressure and bottom pressure to estimate a sea level time series (sea level = bottom pressure – atmospheric pressure), then sea level peaks 30° before bottom pressure and southward geostrophic transport occurs when sea level is falling rapidly, slightly after maximum bottom pressure. As far as we can tell from atmospheric pressure, bottom pressure and barotropic geostrophic transport (not sea level directly), the phasing matches the global 5-day oscillations driven by atmospheric pressure variations described by Hirose et al. (2001). Here at 26° N, the 4–5 day period fluctuations have an rms amplitude in geostrophic transport of about 3.5 Sv with associated sea level variations of 0.5 cm. More observations of sea level and bottom pressure throughout the North Atlantic are needed to refine the understanding of these 4–5 day variations in zonally averaged bottom pressure found here at 26° N.

Acknowledgements. The Rapid monitoring project is jointly supported by the Natural Environmental Research Council (NERC), the National Science Foundation and National Oceanic and Atmospheric Administration. The authors thank NERC for ongoing support of our research efforts. A. Mujahid's PhD studentship was supported by the Malaysian Public Services Department and Universiti Malaysia Sarawak has enabled her continuing contributions to the analysis reported here.

Edited by: A. Sterl

References

Baringer, M. O. and Larsen, J. C.: Sixteen years of Florida Current transport at 27° N, Geophys. Res. Lett., 28, 3179–3182, 2001.

Brown, W., Munk, W., Snodgrass, F., Mofjeld, H., and Zetler, B.: MODE Bottom Experiment, J. Phys. Oceanogr., 5, 75–85, 1975.

Bryden, H. L., Johns, W. E., and Saunders, P. M.: Deep western boundary current east of Abaco: Mean structure and transport, J. Mar. Res., 63, 35–57, 2005.

Chelton, D. B., Schlax, M. G., Samelson, R. M., and de Szoeke, R. A.: Global observations of large oceanic eddies, Geophys. Res. Lett., 34, L15606, doi:10.1029/2007GL030812, 2007.

Cunningham, S. A., Kanzow, T., Rayner, D., Baringer, M. O., Johns, W. E., Marotzke, J., Longworth, H. R., Grant, E. M., Hirschi, J. J.-M., Beal, L. M., Meinen, C. S., and Bryden, H. L.: Temporal Variability of the Atlantic Meridional Overturning Circulation at 26.5° N, Science, 317, 935–938, 2007.

Cunningham, S. A., Rayner, D., and Marotzke, J., et al.: Rapid mooring cruise report April–May 2005, RRS Charles Darwin Cruise CD170 and RV Knorr Cruise KN182-2, National Oceanography Centre Southampton Cruise Report 2, Southampton, UK, 147 pp., 2006.

Hirose, N., Fukumori, I., and Ponte, R. M.: A non-isostatic global sea level response to barometric pressure near 5 days, Geophys. Res. Lett., 28, 2441–2444, 2001.

Johns, W. E., Beal, L. M., Baringer, M. O., Molina, J. R., Cunningham, S. A., Kanzow, T., and Rayner, D.: Variability of shallow and deep western boundary currents off the Bahamas during 2004–05: Results from the 26° N RAPID-MOC Array, J. Phys. Ocean., 38, 605–623, 2008.

Kanzow, T., Cunningham, S. A., Rayner, D., Hirschi, J. J.-M., Johns, W. E., Baringer, M. O., Bryden, H. L., Beal, L. M., Meinen, C. S., and Marotzke, J.: Observed flow compensation associated with the MOC at 26.5° N in the Atlantic, Science, 317, 938–941, 2007.

Kanzow, T., Flechtner, F., Chave, A., Schmidt, R., Schwintzer, P., and Send, U.: Seasonal variation of ocean bottom pressure derived from Gravity Recovery and Climate Experiment (GRACE): Local validation and global patterns, J. Geophys. Res., 110, C09001, doi:10.1029/2004JC002772, 2005.

Kanzow, T., Hirschi, J. J.-M., Meinen, C., Rayner, D., Cunningham, S. A., Marotzke, J., Johns, W. E., Bryden, H. L., Beal, L. M., and Baringer, M. O.: A prototype system for observing the Atlantic meridional overturning circulation – scientific basis, measurement and risk mitigation strategies, and first results, Journal of Operational Oceanography, 1, 19–28, 2008.

Kanzow, T., Johnson, H., Marshall, D., Cunningham, S. A., Hirschi, J. J.-M., Mujahid, A., Bryden, H. L., and Johns, W. E.: Observing basin-wide integrated volume transports in an eddy-filled ocean, J. Phys. Ocean., doi:10.1175/2009JPO4185.1, in press, June 2009.

Kanzow, T., Send, U., Zenk, W., Chave, A., and Rhein, M.: Monitoring the deep integrated deep meridional flow in the tropical North Atlantic: Long-term performance of a geostrophic array, Deep-Sea Res. Pt. I, 53, 528–546, 2006.

Longworth, H. R.: Constraining variability of the Atlantic meridional overturning circulation at 25° N from historical observations, 1980–2005, Ph.D. thesis, School of Ocean and Earth Science, University of Southampton, Southampton, UK, 200 pp., 2007.

Luther, D. S.: Evidence of a 4–6 day barotropic, planetary oscillation in the Pacific Ocean, J. Phys. Oceanogr., 12, 644–657, 1982.

Woodworth, P. L., Windle, S. A., and Vassie, J. M.: Departures from the local inverse barometer model at periods of 5 days in the central South Atlantic, J. Geophys. Res., 100, 18281–18290, 1995.

Wunsch, C.: Mass and volume transport variability in an eddy-filled ocean, Nat. Geosci., 1, 165–168, doi:10.1038/ngeo126, 2008.